Key Points:
- A possible new dust charging effect, the "nanodust shedding," requiring the presence of many small nanometer particles is discussed
- The effect may operate near the Earth's mesopause where cloud particles and large amounts of meteoric smoke particles can coexist
- The effect may explain radar observations of mesospheric clouds showing an unusual reaction to artificial electron heating

Correspondence to:
O. Havnes,
Ove.Havnes@uit.no

Nanodust shedding and its potential influence on dust-related phenomena in the mesosphere

O. Havnes[1] and T. W. Hartquist[2]

[1]Institute of Physics and Technology, Arctic University of Norway, Tromsø, Norway, [2]School of Physics and Astronomy, University of Leeds, Leeds, UK

Abstract We explore the possibility that some meteoric smoke particles that collide with larger nanoparticles near the mesopause can escape from the larger particles by capturing surface electrons. If the process were sufficiently efficient, under certain conditions it would influence the responses of polar mesospheric summer echoes to artificial heating in a manner that is compatible with observations that are unexplained with previous models. The process would have a number of other possible consequences for nanoparticles near the mesopause.

1. Introduction

Noctilucent clouds (NLCs) and the polar mesospheric summer echoes (PMSEs) are optical and radio features, respectively, appearing in the summer polar mesosphere at altitudes of ~80 to ~90 km. The NLC/PMSE dust particles consist mostly of water ice but also contain atomic and molecular meteoric material injected into the upper mesosphere by ablating micrometeoroids [*Hervig et al.*, 2001; *Plane*, 2004; *Lübken and Höffner*, 2004; *She et al.*, 2006]. In addition, they probably contain large numbers of meteoric smoke particles (MSPs) [*Havnes and Naesheim*, 2007; *Hervig et al.*, 2012; *Kassa et al.*, 2012; *Havnes et al.*, 2014].

Dust particles can have a profound influence on the charge balance in the mesosphere [*Pedersen et al.*, 1969; *Havnes et al.*, 1996]. This influence is key to the overshoot effect predicted by *Havnes* [2004] and discovered by *Havnes et al.* [2003] to occur in radar observations of PMSE regions subjected to appropriate time-dependent artificial heating. The heating is accomplished with high-energy transmitters (up to 1.2 MW) in the 3 to 7 MHz range [*Rietveld et al.*, 1993]. Only electrons are heated, and theoretically, the electrons in the mesosphere can be heated up from a few hundred to several thousand degrees Kelvin [*Belova et al.*, 1995]. However, consideration of some of the responses of radar scattering to time-dependent heating of PMSE regions observed by *Havnes et al.* [2015] led to the conclusion that the treatment of dust charging, and its influence on the distribution of gas phase electrons, has possibly been incomplete. Consequently, in this paper we explore how the charges carried by ice particles in PMSE regions may be affected by the attachment of MSPs to the particles and the subsequent ejection of some of the MSPs. Throughout this paper this process is called the "nanodust shedding" effect. We also show that such a process can give rise to radar scattering responses similar to the ones observed by *Havnes et al.* [2015] mentioned above because, as discussed by *Havnes and Kassa* [2009], photodetachment plays a more important role in establishing the charges on small particles than the charges on larger particles.

The proposed nanodust shedding effect has similarities to some "dust cleaning" processes used to remove dust particles that have settled on large surfaces in, for example, plasma production processes [e.g., *Selwyn et al.*, 1990]. *Goree and Sheridan* [1992] and *Flanagan and Goree* [2006] have performed laboratory studies of such shedding effects. However, the experiments are for ejection from large surfaces and for electron temperatures, electric fields, dust sizes, and dust charges that are at least several orders of magnitude larger than those in the mesosphere. For laboratory conditions the rate at which dust particles break off from a large surface is the limiting rate because once a particle is broken off from the larger surface, the repulsive component of the electric force on the attached particle dominates over the attractive polarization component.

However, in the cold summer mesosphere the low charge of the NLC/PMSE particles and associated small repulsive component of the electric force may lead to the polarization component preventing a MSP from being ejected from a NLC/PMSE particle. We propose that in at least one potential nanodust shedding process the time dependence of the polarization component limits the importance of that component and allows the shedding of some charged MSPs. In this particular process a neutral MSP strikes the surface of a

NLC/PMSE particle, picks up one of the electrons on the larger particle, and is ejected by a monopole component of the electric field before the polarization component is induced.

Section 2 contains a summary of key observations of the overshoot effect and models of the effect. In section 3 we consider the number of MSPs that may be embedded within or attached onto the surface of a NLC/PMSE particle and whether any of them can be electrostatically torn off. We further discuss whether a charged MSP that has been torn off can be fully removed from the NLC/PMSE particle or whether a polarization field induced in the NLC/PMSE particle by the MSP will prevent this. In section 4 we study the effects that a nanodust ejection process can have on radar backscatter. Our results are compared with PMSE overshoot observations [*Havnes et al.*, 2015] for cases for which the Mobile Radar and Rocket Observatory (MORRO) and European Incoherent Scatter (EISCAT) VHF radars show unusual and nearly identical reactions to the electron heating. Section 5 contains a discussion of the results and concludes the paper.

2. Key Points Concerning the Overshoot Effect

Havnes et al. [2003] used a heating cycle with 20 s on and 160 s off to create the first overshoot feature. *Havnes* [2004] called the time variation of radar backscatter the "overshoot characteristic curve" (OCC). The "classical" OCC observed with the EISCAT VHF and UHF radars [*Havnes et al.*, 2003; *Kassa et al.*, 2005; *Næsheim et al.*, 2008] is characterized by an abrupt weakening as the heater is switched on [*Chilson et al.*, 2000]. There can be some recovery of the backscatter during the time the heater is kept on. When the heater is initially switched off, one often observes a sudden increase (overshoot) of the backscatter by a factor that can be up to ~6 above the backscatter observed after the subsequent relaxation back to the normal conditions for an unheated region in a steady state [*Kassa et al.*, 2005]. When the heater is switched on, the electrons are heated practically instantaneously but ions and neutrals are not affected. The dust density distribution is assumed to be unaffected by the heating, but the charge carried by the dust will influence the electron density. The heated electrons will initiate two processes: dust will become more charged and the heating of the electrons will affect the plasma density, which will readjust. If readjustment is the faster process, the main effect will be that electron density gradients are weakened and the radar backscatter therefore also weakens. If the charging is the faster process, the increased charges on dust particles can lead to the electrons being forced into forming steeper density gradients causing the radar backscatter to increase. During the time that the heater is on, the dust will continue to be charged. When the heater is switched off, the dust will be more charged than before the heater was switched on and force the now cooler electrons into a distribution with stronger density gradients than before the heater was switched on. This also leads to a stronger radar backscatter—an overshoot.

The initial models for the overshoot effect [*Havnes*, 2004; *Havnes et al.*, 2003; *Biebricher et al.*, 2006] were based on the assumption of an instantaneous adjustment of the electron and ion density when the heater was switched on and off. In addition, the electron and ion densities were described by Boltzmann distributions. The rapid plasma density adjustment caused by the change in dust charging leads to a reduction of electron density gradients and therefore a weakening of the radar backscatter when the heater is switched on and the electrons are heated [*Biebricher and Havnes*, 2012]. In most cases, radar backscatter models based on these assumptions reproduce the overshoot effect observed with high-frequency radars such as the EISCAT VHF (224 MHz) and UHF (930 MHz) [*Næsheim et al.*, 2008; *Biebricher and Havnes*, 2012]. For these radars the most efficient backscatter dust density irregularities, at the Bragg scale lengths, which are half the radar wavelengths, are 67 cm and 16 cm, respectively. For such small dust inhomogeneity dimensions the time required for the plasma density adjustment, caused by electron temperature changes when the heater is switched on or off, will normally be shorter than the dust charging time.

However, for the low-frequency MORRO radar at 56 MHz [*La Hoz and Havnes*, 2008] and EISCAT HF radar at 8 MHz [*Senior et al.*, 2014] the Bragg lengths are 2.7 m and 38 m, respectively, and the plasma adjustment times will often be longer than the dust charging time. Modeling [*Scales*, 2004; *Scales and Chen*, 2008; *Mahmoudian et al.*, 2011; *Mahmoudian and Scales*, 2012] showed that shortly after the heater is switched on, a finite plasma adjustment time can cause a rapid increase of the backscatter signal to a level above that before the heater was switched on. This is due to additional charging of the dust particles occurring as the plasma adjusts and counteracting a plasma density adjustment toward reduced density gradients. Instead, the additional dust charging leads to enhanced electron density gradients and enhanced radar backscatter
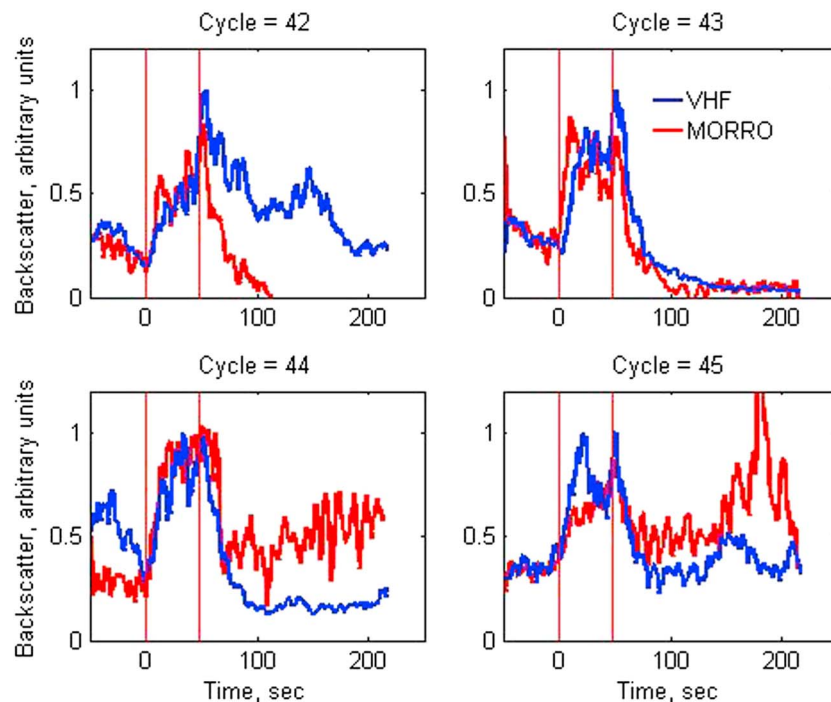
Figure 1. Observations of overshoot cycles 42 to 45 taken with the EISCAT VHF radar (blue curves) and the collocated MORRO radar (red curves). These are observation of a thin layer in the low parts (~82 km) of the PMSE region, taken on 26 July 2013 between 11:49 and 12:00 UT. The heater is on for 48 s and off for 168 s.

shortly after the heater is switched on. Such behavior in OCCs has recently been observed with the EISCAT HF radar [*Senior et al.*, 2014] and also with the MORRO radar and EISCAT VHF radar [*Senior et al.*, 2014; *Havnes et al.*, 2015].

Havnes et al. [2015] found that on average there is a distinct difference between the OCCs observed with the MORRO radar and those observed with the 224 MHz EISCAT VHF radar. This result agrees with numerical modeling of OCCs [*Mahmoudian et al.*, 2011; *Biebricher and Havnes*, 2012]. However, during a PMSE campaign in 2013, on each of a few occasions, simultaneous observations with the two radars yielded very similar OCCs showing exceptionally strong and nearly instantaneous increases after the heater was switched on and a shorter relaxation time than usual after the heater was switched off [*Havnes et al.*, 2015]. Such behavior is seen in the data shown in Figure 1. This behavior was present on 26 July 2013 for only about 15 min out of a total observing time that day of 3.8 h. In Figure 1 we have normalized the VHF backscatter so that the maximum value of it is equal to 1. This occurs near the time when the heater is switched off. We thereafter changed the scale of the MORRO backscatter, so it coincides with the VHF backscatter at the time that the heater is switched on. The original backscatter for the cycles was strongest for cycle 42 and weakened continuously to a minimum at cycle 45.

The modeling referred to above does not predict that the observations obtained with radars differing as much as MORRO and VHF should show the same behavior. Due to differences in the wavelengths, and thus the detected scattering structures, models also show very different OCCs as demonstrated by Figure 1 of *Mahmoudian et al.* [2011] and Figure 12 of *Biebricher and Havnes* [2012]. The fact that for some cases OCCs obtained simultaneously at different frequencies are practically identical led *Senior et al.* [2014] and *Havnes et al.* [2015] to suggest that the models for the charge increase during the time the heater is on could be incomplete.

The suspicion that the present models for dust charging in the mesosphere are not complete is also supported by recent rocket observations obtained with a new dust mass analyzer called Mesospheric Aerosol Sampling Spectrometer (MASS) [*Knappmiller et al.*, 2008]. The results show relatively high density layers of both positively and negatively charged dust particles with sizes of just a few nanometers. These particles coexist with larger

"normal" negatively charged aerosols [*Robertson et al.*, 2009]. Standard charging models normally predict small values of the abundance ratio of such positively charged small particles to neutral and to negatively charged small particles [*Asmus et al.*, 2015] for normal daylight conditions.

3. Ejection of Charged MSPs From the Surfaces of NLC/PMSE Particles

Using data from the Solar Occultation for Ice Experiment instrument on the AIM satellite, *Hervig et al.* [2012] concluded that the volume filling factor, V_f, of MSPs in NLC/PMSE particles is ~0.01% to ~3%. An analysis of data obtained with a rocket-borne impact detector Multiple Dust Detector (MUDD) led *Havnes et al.* [2014] to suggest that the upper limit may possibly be higher if only a small fraction of the volume of an impacting NLC/PMSE particle is fragmented. If $V_f = 3\%$, and the MSP radius is $r = 1$ nm, a NLC/PMSE particle of radius 50 nm will contain 3750 MSPs. The average distance Δ between the MSPs, found from 3750 Δ^3 = volume of the NLC/PMSE particle, is $\Delta = 5.2$ nm. The number of MSPs in a surface layer of a thickness equal to r on a NLC/PMSE particle of radius R, and volume $4\pi R^2 r$, where a fraction $V_f/100$ is made up of embedded MSPs, is $N_S = 3\left(\frac{V_f}{100}\right)(R/r)^2$. The average distance between MSP particles on the surface is $\Delta L_S = (4\pi R^2/N_S)^{1/2}$. For $V_f = 3\%$, $R = 50$ nm, and $r = 1$ nm, $N_S = 225$ and $\Delta L_S = 12$ nm.

The exact structure and shape of a MSP is unknown [*Hervig et al.*, 2012], as is how a MSP initially becomes attached to a larger icy NLC/PMSE particle. However, it is unlikely that a MSP particle, which will collide with a kinetic energy of ~$3k_BT/2$, where k_B is the Boltzmann constant, will bury itself deeply within a NLC/PMSE particle composed of ice. This conclusion is supported by the consideration of the maximum depth, H_S, to which a cylinder with the radius of a MSP can be melted by an input of heat equal to the kinetic energy of a MSP. For $r = 1$ nm, a kinetic temperature of 150 K, and heat of sublimation of 3.34×10^5 J/kg we find a "penetration" depth of $H_S \sim 10^{-3}$ nm, which is less than the size of an ice molecule. Although some deformation of the NLC/PMSE particle surface and MSP surface may occur, we can safely assume that in a MSP-NLC particle collision, the MSP will not become part of a smooth NLC particle surface. Instead, if the MSP is spherical, it will protrude from the general surface a distance that is not much less than the MSP diameter $2r$. If the MSP surface is characterized by protruding features, the distance that the MSP extends from the NLC/PMSE particle surface could be larger. The initial area of the contact surface is uncertain. However, unless the MSP detaches too quickly, the contact area will grow as water vapor condenses and freezes onto the surface of the NLC/PMSE particle, creating a contact bridge until the MSP is covered and fully embedded.

A vital question concerns whether the ejection of an attached MSP can occur from a NLC/PMSE particle of a specified charge. Since NLC/PMSE particles seem to have many MSPs embedded in them, the detachment of MSPs should often be slower than MSP attachment. However, as we will show later, smaller MSPs probably have a higher probability to be ejected than the larger ones. It is therefore possible that the size distribution of embedded MSPs can differ from the ambient MSP size distribution.

Electrostatic disruption, by which a part of a dust particle is torn off, occurs when the electrostatic outward force per unit surface element becomes larger than the tensile strength of the particle [e.g., *Öpik*, 1956; *Mendis and Horányi*, 2013]. Normally, this process is considered for environments with comparatively high plasma temperatures and containing micron-sized or larger dust particles, which carry large charges. This is not the case in the low-temperature and weakly ionized gas of the middle atmosphere. At the NLC/PMSE altitudes the summer plasma and neutral temperatures are of the order of 150 K [*Lübken et al.*, 2002]. Theoretically, artificial electron heating may raise the electron temperature to above 2000 K [*Belova et al.*, 1995; *Kero et al.*, 2000], but normally, the heating-induced temperature in the NLC/PMSE region is much less than this [*Kassa et al.*, 2005]. Even at these elevated electron temperatures, the numbers of charges on NLC/PMSE particles are still low as shown in Figure 2.

If a NLC/PMSE particle has two or more electrons, the force that they exert on each other could cause each of them to be positioned on the NLC/PMSE particle surface, possibly on a protruding MSP. An electron may not easily leave a MSP until the MSP becomes well embedded in the NLC/PMSE particle by condensing and freezing water. For some number, greater than 1, of electrons on a NLC/PMSE particle, the electric field may be strong enough that a surface MSP containing an electron is torn off. As we will discuss later, this by itself is a necessary but insufficient condition that the charged MSP particle will leave the NLC/PMSE particle. In Figure 2 we show the equilibrium charge distributions for three different dust sizes and for two different
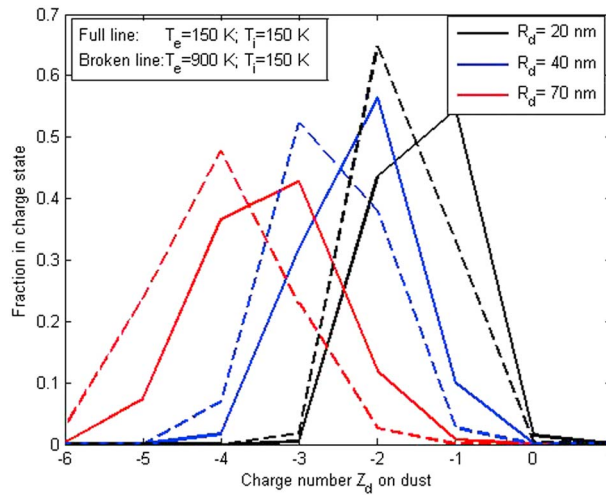
Figure 2. The equilibrium charge distribution for three different NLC/PMSE particle sizes and for two different electron temperatures. The NLC/PMSE particle charge density is assumed to be small compared to the charge density of the gas phase electrons.

electron temperatures. Charging is assumed to be due only to electron and molecular ion collisions with the NLC/PMSE particles. The charge number per NLC/PMSE particle ranges from $Z_d = -1$ to -6 for the assumed sizes. For simplicity, henceforth, we will assume that the electric field due to the charges on a NLC/PMSE particle is that of a monopole at the center of the particle.

Before the contribution to the force due to polarization can develop, the radial force from the NLC/PMSE particle of charge number Z_d, on a MSP attached to its surface and having a charge $q = -e$, is simply that associated with an electric monopole and is given by

$$F_{\text{out}} = \frac{|Z_d|e^2}{4\pi\epsilon_0 R^2} = 2.3 \times 10^{-10} |Z_d|/R(\text{nm})^2 \quad , \text{N} \tag{1}$$

Here R is the NLC/PMSE particle radius, $\epsilon_0 = 8.85 \times 10^{-12}$, F/m is the permittivity of free space, and e is the elementary charge. We have neglected any attraction due to a polarization component of the force between a charged protruding MSP and the charge distribution that it has induced on the NLC/PMSE particle. In steady state, this attractive component will be approximately a factor $(R/r)^2/|Z_d|$ larger than the outward component given by equation (1). Thus, for a typical low NLC/PMSE charge, in steady state equilibrium the polarization component will keep the MSP attached to the NLC/PMSE particle. In the following we consider a scenario, which we describe in section 3.2 and in which the induced charge distribution on the NLC/PMSE particle may not be in steady state equilibrium. This leads the polarization component to be negligible and to MSP ejection.

We now focus on whether the monopole component of the electric repulsive force F_{out}, in the absence of a polarization component, can tear a singly negatively charged MSP from a NLC/PMSE particle. We assume the contact area to be a fraction γ of the MSP cross section πr^2. This gives for the tensile force f_E, the electric repulsive force per unit area, in the contact bridge between the MSP and the NLC/PMSE particle

$$f_E = \frac{F_{\text{out}}}{\gamma r^2} = 7.4 \times 10^7 |Z_d|/\gamma r(\text{nm})^2 R(\text{nm})^2 \quad , \text{Pa} \tag{2}$$

For NLC/PMSE sizes and charge numbers (R, Z_d) of (40 nm, -3) and (70 nm, -6), $r = 1$ nm, and γ between 1 and 0.1, the tensile force f_E will be about 6×10^4 to a few times 10^6 Pa. For the smallest MSPs of around 0.3 nm [*Megner et al.*, 2006] the tensile force may be an order of magnitude larger than this.

Debrincat et al. [2008] found that agglomerates of nickel and dust that formed in gravitational free fall have tensile strengths of less than ~40 Pa. Thus, the monopole component of the electric force on a charged MSP that has only recently attached to a NCL/PMSE particle may be larger than the tensile strength of the MSP. However, as mentioned above, an icy contact bridge between a MSP and the surface of a NLC/PMSE particle may grow and finally cause the MSP to be entirely embedded. A contact bridge will probably consist of ice in a form affected by the impact of the MSP, in addition to factors like metallic impurity components, surface effects, the embedded MSP, and internal reorganization, all of which may influence the material strength [*Bartels-Rausch et al.*, 2012]. The bridge and its tensile strength may therefore differ significantly from that of pure ice. For loose ice aggregates, the tensile strength f_t can be ~10^3 Pa [*Grün et al.*, 1984]. For ice similar to that in comets, with a density ρ ~ 250–300 kg/m^3, values of f_t may range from 10^3 to 10^4 Pa [*Pat-El et al.*, 2009; *Seizinger et al.*, 2013]. For ice of density ~900 kg/m^3 the tensile strength under tension is a factor 3–5 lower than under compression and is a few times 10^6 Pa [*Lange and Ahrens*, 1983]. The measurements for this
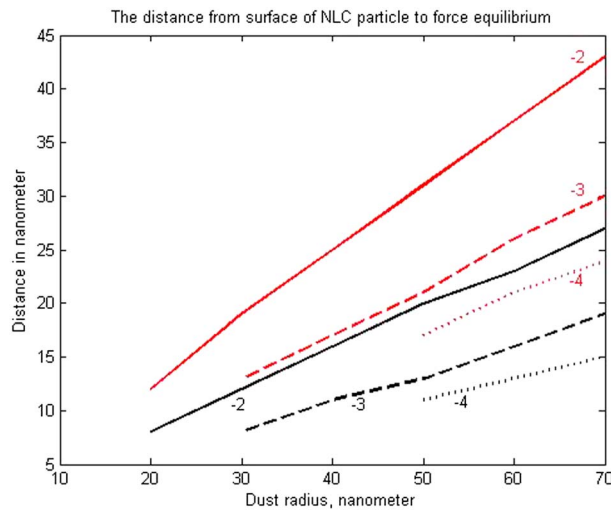
Figure 3. The distance from the surface of a NLC/PMSE particle where the attractive and repelling components of the force are equal. The black curves are for $\varepsilon = 3.2$ and the red for a conductor ($\varepsilon = \infty$). The numbers in the figure are the charge numbers (cf. Figure 2) for substantial fractions of the NLC/PMSE particles.

final type of ice were made at 264 K, while the mesospheric ice particles are at ~150 K. The strength of ice normally increases with falling temperatures [*Litwin et al.*, 2012], so we cannot exclude the possibility that pure ice at NLC/PMSE conditions may have a considerably larger tensile strength than quoted here.

Though uncertainties exist, there seems to be a reasonable chance that under some conditions the monopole component of the tensile force on a surface MSP containing an electron is sufficiently large to tear the whole MSP, or part of it, from a NLC/PMSE particle.

3.1. Can a Torn Off Charged MSP Escape From a NLC/PMSE Particle?

The disruption of the contact between a NLC/PMSE particle and a charged MSP does not guarantee that the MSP will escape. Polarization effects may produce a net attractive force at close distances. The interaction between two finite-sized charged spheres with different electrical characteristics (e.g., conductor or dielectric), sizes, and charges has been extensively studied. Depending on the conditions, the interparticle force can be attractive or repulsive even if the two particles have charges of the same sign [e. g. *Feng*, 2000; *Konopka et al.*, 2000; *Markes and Williams*, 2000; *Filippov*, 2009; *Kolikov et al.*, 2012; *Munirov and Filippov*, 2013].

The situation that we consider resembles that of a small point-like charge (the charged MSP) near a large particle (the NLC/PMSE particle) carrying a charge of the same sign. In such a case, in steady state the interparticle force is attractive when the MSP is sufficiently close to the NLC/PMSE particle and repulsive when the particles are sufficiently separated [e.g., *Jackson*, 1962; *Batygin and Toptygin*, 1978]. For steady state, *Draine and Sutin* [1987] find that the interaction potential U_I, due to the charge $Q = Z_d e$ on the NLC/PMSE particle and the charge induced by the MSP at a distance x from the center of the dielectric NLC/PMSE particle, can be approximated by

$$U_I(x) = \frac{qQ}{x} - \left(\frac{\varepsilon - 1}{\epsilon + 2}\right) \frac{q^2 R^3}{2x^2\left(x^2 - R^2\right)}. \tag{3}$$

Here the charge of the MSP is $q = -e$ and the dielectric constant of the NLC/PMSE particle is ε. The remaining NLC/PMSE particle charge, after a charged MSP has been broken off, is $Q = (Z_d + 1)e$. Using a dielectric constant for ice of $\varepsilon = 3.2$ [*Evans*, 1965; *Warren*, 1984], we calculate the distance $x_0 = x - R$ from the surface of the NLC/PMSE particle where $U(x)$ has its maximum and show the results in Figure 3. Inside this distance the two particles attract each other, while at larger distances they repel each other. For $(R, Z_d) = (20 \, \text{nm}, -2), (40 \, \text{nm}, -3)$, and $(70 \, \text{nm}, -4)$, the respective equilibrium distances x_0 are 8, 11, and 15 nm outside the surface of the NLC/PMSE particle.

However, an attractive polarization component of the field will not initially exist if just before the start of the disruption process the MSP attached to the NLC/PMSE particle surface is neutral. If an electron travels at the thermal speed, it covers 1 nm in about 10^{-14} s, and the capture of an electron by a MSP and the establishment of the monopole component of the force must occur on a comparable timescale. Consequently, the MSP is torn from the surface if the polarization component is not established just as rapidly. The MSP will escape entirely from the larger particle if the monopole component of the force drives it to a distance greater than x_0 before the polarization component is established. We take v to be the radial component of the MSP
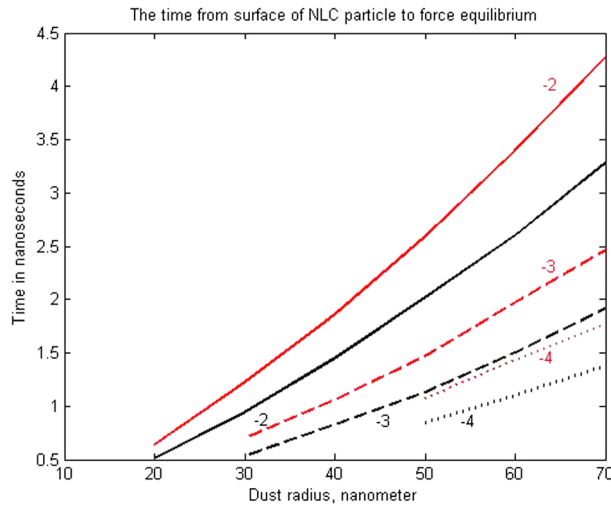
Figure 4. The time for a MSP to move from the surface of a NLC/PMSE particle to the equilibrium point, beyond which the steady state force is repulsive. Black curves are for a dielectric NLC/PMSE particle, and red curves are for a conducting one. The numbers on the curves are the charge numbers of the NLC/PMSE particle.

velocity and integrate $m_{msp}(dv/dt) = -Qe/4\pi\varepsilon_o x^2$ to find the time t_0 for a MSP of radius $r = 1$ nm and mass $m_{msp} = 8.4 \times 10^{-24}$ kg to move from the surface at $x = R$ to a distance $x = R + x_0$ from the center of the NLC/PMSE particle. Figure 4 shows the results for t_0. For dielectric NLC/PMSE particles the times t_0 are 0.5, 0.7, and 1.4 ns for NLC/PMSE particles of radii 20, 40, and 70 nm, respectively. If the MSP size is reduced by a factor 2 to $r = 0.5$ nm, the respective times are reduced by a factor of almost $\sqrt{8}$ to 0.2, 0.3, and 0.5 ns.

To our knowledge, no estimates of the time scale for establishing polarization in small nanometer-sized NLC/PMSE particles exist. However, we note that in other cases in which polarization effects are important, typical times for polarization switching are often considerably longer than the times t_0 found above. For ferroelectric thin (e.g., ~35 nm) films the polarization switching times are from tens to hundreds of nanoseconds [*Grigoriev et al.*, 2009]. *Hazarika and Kumar* [2014] found that the relaxation time for charge carriers in polymers can be more than 100 ns at room temperature and increase at lower temperatures. For ceramic plates of thickness 1 mm and applied switching field strengths of a few kV/mm, *Zhukov et al.* [2014] found relaxation times ranging from milliseconds to many seconds, depending on the material and grain size in the ceramic. For larger switching fields of 20 to 35 kV/mm they found relaxation times between 10^{-11} and 10^{-10} s for all the investigated materials. The field at the surface of the NLC/PMSE grain produced by its own charges will be a few kV/mm, if the breaking off of the charged MSP does not produce a substantial local field on the part of the surface of the NLC/PMSE closest to it. Although the cited experiments are for material properties and conditions that differ from what we can expect for NLC/PMSE particles, it appears likely that the time to establish the polarization component of the field of the NLC/PMSE particle can be long enough to allow a charged and broken off MSP to escape. Below we will assume this to be the case.

3.2. The Assumed Parameterization of the MSP Ejection Rate

The photodetachment of electrons causes the large majority of free MSPs to be neutral [*Havnes and Kassa*, 2009; *Rapp*, 2009], and in the scenario that we consider NLC/PMSE particles accrete neutral MSPs [*Havnes and Naesheim*, 2007]. If a loosely attached MSP that has not become well embedded by ice becomes charged, it may be torn off by the NLC/PMSE particle surface and escape. The least embedded attached MSPs will be those that have attached most recently, and electrons are more likely to remain bound to such MSPs than to well-embedded MSPs, which are better connected to the surrounding ice. The protrusion of a newly attached MSP above the NLC/PMSE surface may lead it to have a nonnegligible probability of capturing an electron that is moving freely over the surface.

Given the grounds for supposing that the MSPs that are most likely to be ejected are the MSPs that have become attached recently, we assume that the MSP ejection rate is a simple function of the attachment rate. In this paper, we take the ejection rate to be a constant fraction ξ of the attachment rate, which is given by

$$\frac{dN_{msp,a}}{dt} = \pi R^2 n_{msp} v_{msp}. \qquad (4)$$

We here assume that all impacting MSPs will attach and that practically all MSPs are neutral [*Havnes and Kassa*, 2009]. The number density of MSPs in the NLC/PMSE cloud is n_{msp}. Their average impact speed onto the NLC/PMSE particle is $v_{msp} = (8k_B T_N/\pi m_{msp})^{1/2}$ where T_N is the neutral gas temperature.

4. The Consequences of the Shedding for the Overshoot Effect

The inclusion of the nanodust shedding mechanism in an overshoot model and the comparison of model results and observational results are relatively straightforward.

4.1. Inclusion of the Nanodust Shedding Effect in the Overshoot Model

Our description of the varying mesospheric dusty plasma, in our case the main dust being NLC/PMSE particles, during a heater cycle is based on a model introduced by *Havnes and Morfill* [1984] and *Havnes* [2004]. The plasma is assumed to react instantaneously to changes in electron temperature, and the local plasma densities n have Boltzmann distributions so that

$$n_\alpha = n_0 \exp(eV/kT_\alpha) \quad \alpha = e, i. \tag{5}$$

A dust structure associated with radar backscatter is assumed to have a central dust density that is some fraction above or below the average background dust density n_d in the general dust layer [e.g., *Biebricher et al.*, 2006]. Outside that general layer the dust density is zero, the local plasma potential V is also zero, and the electron and ion number densities are both equal to n_0. The electron, ion, and neutral temperatures are T_e, T_i, and T_N, respectively. When the heater is off, $T_e = T_i = T_N$, but when it is on, $T_e > T_i = T_N$. We assume that when the electron temperature changes, the redistribution of electrons and ions is instantaneous. We show how the nanodust shedding effect, if active, can have a considerable influence on the OCCs for radars operating over a broad frequency range. A key result is the demonstration that the inclusion of the nanodust shedding effect can lead to OCCs at VHF and UHF, as well as at lower frequencies, which show, after the heating has been switched on, brief reductions in backscatter followed by simultaneous rapid and strong radar backscatter increases.

We assume that the charge on a NLC/PMSE particle changes continuously. This approximation for the NLC/PMSE is acceptable as long as its charge number $|Z_d| > 1$. We neglect the charge distribution shown in Figure 2 and take all NLC/PMSE particles to have the same R and Z_d. Z_d is governed by

$$\frac{dZ_d}{dt} = -J_e + J_i + \xi \pi R^2 n_{\text{msp}} v_{\text{msp}} \tag{6}$$

J_e and J_i are the fluxes of electrons and ions, respectively, onto a NLC/PMSE particle. The last term of equation (6) is due to a fraction ξ of the neutral MSPs that attach to the NLC/PMS particle are scavenging electrons from it and being re-ejected. J_e is given by

$$J_e = \pi R^2 n_0 s_e (8k_B T_e/\pi m_e)^{1/2} \exp(e(U + V)/k_B T_e) \tag{7}$$

where the surface potential U of a NLC/PMSE particle is

$$U = Z_d e / 4\pi \varepsilon_0 R \tag{8}$$

and s_e is the sticking coefficient for an electron. The ion flux is

$$J_i = \pi R^2 n_0 (8k_B T_i/\pi m_i)^{\frac{1}{2}} \exp\left(-\frac{eV}{k_B T_i}\right)\left(1 - \frac{eU}{k_B T_i}\right) \tag{9}$$

if each ion is singly ionized and the ion sticking coefficient is 1.

Quasi-neutrality demands that the charge densities of electrons, ions, NLC/PMSE, and MSPs sum to zero.

$$-n_e + n_i + Z_d n_d - N_{ej}^- n_d = 0 . \tag{10}$$

N_{ej}^- is the number of MSPs, per NLC/PMSE particle, that are negatively charged. We do not include positively charged MSPs, which we assume to have a number density much less than that of the negatively charged MSPs. N_{ej}^- is governed by

$$\frac{dN_{ej}^-}{dt} = j_e - N_{ej}^- D + \xi \pi R^2 n_{\text{msp}} v_{\text{msp}} \tag{11}$$

Here j_e is the attachment rate of electrons to a neutral MSP. This flux will be given by the equations (7) with the NLC/PMSE particle radius R replaced by the MSP radius r and the surface potential $U = 0$. D is the rate for photodetachment, which in our cases dominates over ion attachment and other processes that neutralize negatively charged MSPs smaller than a few nanometers [*Havnes and Kassa*, 2009; *Rapp*, 2009]. During
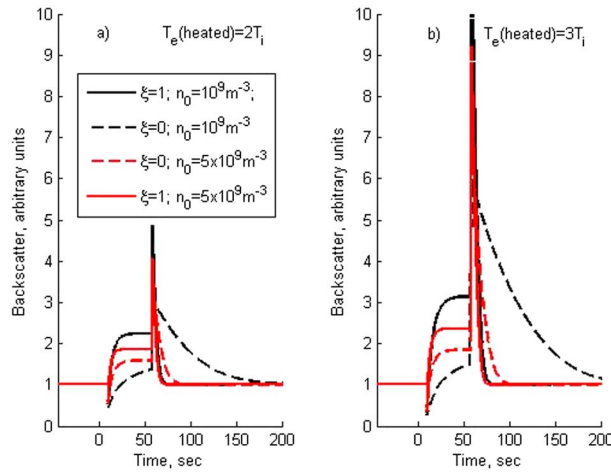
Figure 5. Model results showing dependence of OCC on the shedding efficiency ξ, the background electron and ion density n_0, and the amount by which the electrons are heated. For both figures the NLC/PMSE radius and density are 70 nm and $n_d = 10^7\,\text{m}^{-3}$, respectively, $r = 0.5$ nm, $n_{\text{msp}} = 2 \times 10^{11}\,\text{m}^{-3}$, $T_e(\text{cold}) = T_i = 150$ K, and the photodetachment coefficient $D = 3$. The legends shown in Figure 5a also apply to Figure 5b.

daylight D for a 0.5 nm MSP could be from ~5 to ~0.1 el s^{-1} per MSP for a work function from ~3 to ~6 eV [*Havnes and Kassa*, 2009], while the ion flux to neutralize a MSP is in the range 10^{-4} to $10^{-3}\,\text{s}^{-1}$ per MSP for ion densities between 10^9 and $10^{10}\,\text{m}^{-3}$. The photodetachment term can also be used to represent the effect of diffusion on the spatial density distribution of the ejected charged MSPs. Recently ejected MSPs will have an initial density distribution with a shape similar to that of the NLC/PMSE particles, but diffusion will lead to a loss of charged MSPs out of the region containing a high density of the NLC/PMSE particles. Diffusion should be more significant for structures scattering the highest frequencies, such as the EISCAT UHF, which consequently may show a smaller backscatter increase after the heater is turned on than the VHF and MORRO do.

The radar reflection coefficient is proportional to the electron density gradient squared [*Ginsburg*, 1964]. Thus, as in earlier work [e.g., *Kassa et al.*, 2005; *Biebricher et al.*, 2006], we take the relative backscatter $B(t)$ at a fixed frequency as a function of time to be

$$B(t) = \left(\frac{n_{ec}(t) - n_{e0}(t)}{n_{ec}(0) - n_{e0}(0)} \right)^2 . \tag{12}$$

Here $n_{ec}(t)$ and $n_{eo}(t)$ are the time-dependent electron number density at the center of the dust clump and in the general dust background, respectively. Time $t = 0$ refers to the time just before the heater is switched on, and the backscatter $B(t)$ is given relative to the backscatter at $t = 0$.

4.2. Model Results and Comparison With Observations

We have used the model to study the dependence of the OCC on ξ and have limited our modeled cases to those for which results are shown in Figure 5. We have assumed a heating cycle with a relatively short heating on time and a much longer heater off time, so the dusty plasma can relax back to its unperturbed state. The OCCs for the model for which the nanodust shedding effect is not active ($\xi = 0$) are shown with a broken lines. We have calculated OCCs for two different electron and ion density n_0 and for two different heated electron temperatures. We see that for larger electron densities the effect of nanodust shedding is decreased and the two OCCs for $\xi = 0$ and $\xi = 1$ approach each other. The nanodust shedding will not be effective for small NLC/PMSE below approximately 20 nm where the average charge number approach $Z_d = -1$.

We see that the OCC is a sensitive function of ξ. The most characteristic feature of the $\xi \neq 0$ cases when the electron density is low is the rapid increase in backscatter shortly after the heater is switched on. As mentioned in section 2, similar behavior is also apparent in models including finite plasma adjustment times [*Scales*, 2004; *Biebricher and Havnes*, 2012] and is present in the observed cases for which results are shown in Figure 1. Without a nanodust shedding effect, the recovery of the backscatter will be very much slower and weaker which apparently does not describe these observations.

The more rapid and larger increase of the backscatter when the heating is first switched on in models including the nanodust shedding is due to that process lowering the magnitude of the negative charges on the NLC/PMSE particles before the heater is switched on. Therefore, when the electrons are heated, they can deliver more extra charges to the NLC/PMSE particles than when the nanodust shedding effect is not active.

The scavenging of NLC/PMSE charges by accreted MSPs and the subsequent ejection proceed at a rate that in our models is unaffected by the electron temperature, since the electron flux dominates over the neutral MSP flux to a NLC particle, while the shedding effect is proportional to the attachment rate of neutral MSP to the NLC/PMSE particles. Consequently, the change in the total space charge in a dust scattering feature, during the time that the electrons are heated, can be much larger when nanodust shedding is included.

We see that the observed OCCs of Figure 1 show very moderate immediate overshoots when the heater is switched off at $t = 48$ s but the increase with respect to the OCC preheating level is considerable. The results of our model show higher and very narrow overshoot peaks when the nanodust shedding effect is important. Much, but maybe not all, of the difference between the observations and our model results may be due to our neglect of finite plasma adjustment times. In overshoot experiments this effect [*Scales*, 2004] will change the OCC especially when the heater is switched on and off. Since the finite adjustment time leads to a less rapid change of electron density, this effect will tend to smear out and lower the overshoot peaks. The generally lower overshoot peaks for the MORRO observations are consistent with the plasma adjustment time being longer for the MORRO scattering structures than for the VHF scattering structures.

It is difficult to estimate accurately the OCC relaxation time, the time required when the heater is switched off for the backscatter to return to its undisturbed level. However, it is clear from Figure 1 that the relaxation times for these rare cases tend to be considerably shorter than for cases showing the classical overshoot with a clear and prolonged reduction in backscatter after the heater is switched on. For other layers present on the same day as the observations summarized in Figure 1 were taken, the relaxation times ranged up to and above 100 s [*Havnes et al.*, 2015]. The data represented in Figure 1 indicate relaxation times as low as 20–30 s. The relaxation time for Figure 5 models without nanodust shedding, but with similar parameters to models including nanodust shedding which qualitatively reproduce the rapid and large increase shortly after the heater was turned on, has a relaxation time from 100 s. For higher plasma densities this relaxation time will be reduced and so will the magnitude of the recovery after the heater is switched on. However, when the observations were obtained, the electron density was probably not very high since ~30 min later, a PMSE layer at 86 km appeared and showed a strong response when the heater was switched on. Such a response requires relatively low electron densities at lower altitudes to avoid strong absorption of the heater wave before it reaches the high layer [*Kassa et al.*, 2005]. In *Havnes et al.* [2011] the influence of horizontal winds on the relaxation time for PMWE was discussed and it was found that winds in excess of 100 m/s were required to explain the observed relaxation times of ~60 s. For the cases of the present paper, with much shorter relaxation times, winds of more than 200 m/s would have been required. In addition, if winds were responsible for the short relaxation time of ~20 to 30 s, we should have seen a clear difference between the relaxation times observed with the 56 MHz MORRO radar and the 224 MHz VHF radar due to their very different beam widths of ~8 km and ~1.5 km, respectively. Such differences are not apparent in Figure 1.

Our model is able to reproduce the short relaxation times, but a large MSP density is required. Short model relaxation times are due to the combination of a rapid reduction of the NLC/PMSE particle charges by the nanodust shedding and a rapid neutralization of ejected charged MSPs by photodetachment.

5. Discussion and Conclusions

If the proposed nanodust shedding effect is important in the mesosphere, the MSPs play more active roles than previously thought.

In the absence of a nanodust shedding effect, at normal mesospheric conditions neutral MSPs will become attached to NLC/PMSE particles and become embedded in them as they grow [*Havnes and Naesheim*, 2007; *Hervig et al.*, 2012]. The MSPs will eventually be returned to the ambient medium when the NLC/PMSE particles sink and evaporate, normally in the lower parts of the NLC/PMSE region. However, this picture will be modified if under some conditions nanodust shedding is sufficiently effective that a considerable fraction of the accreted MSPs are re-ejected. If this is the case, the smaller MSPs may be preferentially re-ejected since they are the ones that tend to have the shortest transport times (cf. Figure 4) from a NLC/PMSE surface to distances exceeding the force equilibrium distance. They should therefore be the least affected by polarization forces, which may attract a MSP back to a NLC/PMSE surface. Variation in the effectiveness of a dust shedding mechanism may be part of the explanation for the observational results of *Hervig et al.* [2012] who found volume filling factors of MSPs in NLC/PMSE particles varying from 3% to 0.01%. By studying

collision fragments of NLC/PMSE particles with a new dust detector MUDD, *Havnes et al.* [2014] and *Antonsen and Havnes* [2015] found that if the particles are embedded MSPs, larger MSPs seem to be overabundant. This may be a consequence of the smaller MSPs having the largest ejection probabilities.

Variation in the efficiency of nanodust shedding may be due to variation in the growth rate of large NLC/PMSE particles arising from differences in atmospheric water content. A large growth rate would lead to an accreted MSP becoming quickly embedded and incapable of acting as an electron scavenger, whereas a low growth rate may allow scavenging and re-ejection.

Variation in the nanodust shedding might also be due to differences in the composition of the icy surfaces of the NLC/PMSE particles, which are expected to contain some material other than pure water ice. Variation in the abundance of such material likely leads, at least occasionally, to the tensile strength to be considerably smaller than that of pure ice. Initially, before condensing and freezing, water vapor establishes a contact bridge, the van der Waals force between a MSP and a NLC/PMSE particle could be dominant, and the composition can affect this force. Calculating it with the Hamaker model [e.g., *Flanagan and Goree*, 2006; *Debrincat et al.*, 2008], we find that for the NLC/PMSE sizes and the MSP size that we have considered, the van der Waals force can be in the interval from 10^{-13} N to a few times 10^{-11} N. The span in magnitude is mostly due to uncertainties in the Hamaker constant, which is typically in the range 10^{-21}–10^{-19} J [*Debrincat et al.*, 2008]. Another critical input parameter in the van der Waals force expression is the distance h between the NLC/PMSE and MSP surfaces. Anticipating that a MSP may be kept at some distance from a NLC/PMSE surface by protruding structures, we have used $h = 1$ nm. The van der Waals force is proportional to h^{-2}. The repelling electric force on a MSP for NLC/PMSE particles of radius from 20 to 70 nm is between 10^{-13} and 10^{-12} N, which is within but at the low end of the van der Waals force range.

Variation in the surface structures of MSPs may also lead to the variation of the ejection efficiency. For example, the tensile strength will be affected if protruding structures, possibly created during agglomeration during MSP growth, on MSPs connect these particles to the NLC/PMSE particles. If the low tensile strengths measured for some agglomerates [*Debrincat et al.*, 2008] are relevant for protruding structures on MSPs, they should be relatively easily broken off in an ejection process and lead to the re-ejection of most or parts of an accreted MSP.

For the nanodust shedding process to have an effect comparable in significance to that of electron impacts, ξ in equations (6) and (11) must not be very small compared to unity. In addition, for the proposed nanodust shedding process to affect the results shown in Figure 5 significantly, the MSP number density, n_{msp}, must be larger than those given by the models of *Hunten et al.* [1980] and *Megner et al.* [2006]. However, overshoot profiles like those shown in Figure 1 are rarely seen. This is probably an indication that the conditions necessary for creating such profiles are also rare. Even if such overshoot cases are unusual, the nanodust shedding effect can still be a factor in determining NLC/PMSE charges and in shaping OCCs for lower MSP densities. We find it plausible that the special cases of low-altitude PMSEs shown in Figure 1 are caused by large NLC/PMSE particles which are affected by sublimation and therefore are returning embedded MSP to the ambient gas and creating an environment with exceptionally high MSP density. We also find that the nanodust shedding may be a factor in maintaining a sufficiently high number density of small MSPs in the mesopause region, where they probably are required as condensation sites for the larger icy NLC/PMSE cloud particles. We are at present unable to determine to what degree a shedding effect will affect the MSP size distribution, due to a lack of knowledge of the many factors which are involved. It is, however, possible that without MSP injection processes such as nanodust shedding, the MSP density in the summer may be too low to explain the observed NLC/PMSE clouds [*Megner et al.*, 2008; *Bardeen et al.*, 2010].

Our primary conclusion is that if it is efficient, nanodust shedding can cause large increases in radar reflectivity at the onset of heating like those shown in Figure 1. However, the proposed nanodust shedding effect may also influence other processes, including those mentioned below.

1. If an accreted MSP has some or many loosely bound parts, the shedding effect may chip off parts of it, which could maintain a high enough abundance of the seed particles required for new NLC/PMSE particles to form. The critical radius, which is the minimum radius that a particle can have and still act as a condensation nucleus, is very temperature dependent and may be down close to 0.5 nm for neutral gas temperatures $\leq$120 K. For higher temperatures the critical radius rapidly increases [*Megner et al.*, 2008].

The shedding effect on the seed particle density should therefore be most effective at low neutral gas temperatures and high water mixing ratios.

2. The dust shedding effect should most effectively shed small MSPs and may therefore lead to an overre-presentation of large MSPs embedded in NLC/PMSE particles.

3. The overshoot relaxation time is the time that passes between the heater turn off and the relaxation of dusty plasma conditions back to those of the undisturbed state. Like the shape of the PMSE overshoots (OCCs), the overshoot relaxation time observed with one radar system will differ for different mesospheric and dust conditions. Without a dust shedding effect the relaxation time depends mainly on the ion density and mass and is most often in the range of 60–100 s [*Havnes et al.*, 2015]. However, in the cases for which results are shown in Figure 1 the relaxation time appears to be much shorter than this. A relaxation time, as observed, down to or less than ~20 to 30 s can be explained if the MSP density is high and if a two-step nanometer dust shedding effect first rapidly removes the excess NLC/PMSE negative charges and thereafter photodetachment neutralizes the ejected MSPs [*Havnes and Kassa*, 2009].

4. The variation from 0.01% to 3% of the observed volume filling factor, V_f, for MSPs within NLC/PMSE particles is easily explained by the variation of the MSP density in the medium from which the NLC/PMSE particles accrete MSPs. However, variation in the efficiency of the nanodust shedding effect will also contribute to large differences in V_f, even if the MSP density does not vary much.

References

Antonsen, T., and O. Havnes (2015), On the detection of mesospheric meteoric smoke particles embedded in noctilucent cloud particles with rocket-borne dust probes, *Rev. Sci. Instrum.*, *86*(3), 12.

Asmus, H., S. Robertson, S. Dickson, M. Friedrich, and L. Megner (2015), Charge balance for the mesosphere with meteoric dust particles, *J. Atmos. Sol. Terr. Phys.*, *127*, 137–149.

Bardeen, C. G., O. B. Toon, E. J. Jensen, M. E. Hervig, C. E. Randall, S. Benze, D. R. Marsh, and A. Merkel (2010), Numerical simulations of the three-dimensional distribution of polar mesospheric clouds and comparison with Cloud Imaging and Particle Size (CIPS) experiment and the Solar Occultation For Ice Experiment (SOFIE) observations, *J. Geophys. Res.*, *115*, D10204, doi:10.1029/2009JD012451.

Bartels-Rausch, T., et al. (2012), Ice structures, patterns, and processes: A view across the icefields, *Rev. Mod. Phys.*, *84*(2), 885–944.

Batygin, V. V., and I. N. Toptygin (1978), *Problems in Electrodynamics*, 2nd ed., Academic Press Inc, London.

Belova, E. G., A. B. Pashin, and W. B. Lyatsky (1995), Passage of a powerful HF radio wave through the lower ionosphere as a function of initial electron density profiles, *J. Atmos. Terr. Phys.*, *57*(3), 265–272.

Biebricher, A., and O. Havnes (2012), Non-equilibrium modeling of the PMSE Overshoot Effect revisited: A comprehensive study, *J. Plasma Phys.*, *78*, 303–319.

Biebricher, A., O. Havnes, T. W. Hartquist, and C. LaHoz (2006), On the influence of plasma absorption by dust on the PMSE overshoot effect, *Adv. Space Res.*, *38*(11), 2541–2550.

Chilson, P. B., E. Belova, M. T. Rietveld, S. Kirkwood, and U. P. Hoppe (2000), First artificially induced modulation of PMSE using the EISCAT heating facility, *Geophys. Res. Lett.*, *27*(23), 3801–3804, doi:10.1029/2000GL011897.

Debrincat, D. P., C. B. Solnordal, and J. S. J. Van Deventer (2008), Characterisation of inter-particle forces within agglomerated metallurgical powders, *Powder Technol.*, *182*(3), 388–397.

Draine, B. T., and B. Sutin (1987), Collisional charging of interstellar grains, *Astrophys. J.*, *320*(2), 803–817.

Evans, S. (1965), Dielectric properties of ice and snow—A review, *J. Glaciol.*, *5*, 773–792.

Feng, J. Q. (2000), Electrostatic interaction between two charged dielectric spheres in contact, *Phys. Rev. E*, *62*(2), 2891–2897.

Filippov, A. V. (2009), Effect of the size of macroparticles on their electrostatic interaction in a plasma, *J. Exp. Theor. Phys.*, *109*(3), 516–529.

Flanagan, T. M., and J. Goree (2006), Dust release from surfaces exposed to plasma, *Phys. Plasmas*, *13*(12), 11.

Ginsburg, V. L. (1964), *The Propagation of Electromagnetic Waves in Plasmas*, Pergamon Press, London.

Goree, J., and T. E. Sheridan (1992), Particulate release from surfaces exposed to a plasma, *J. Vac. Sci. Technol. A-Vac. Surf. Films*, *10*(6), 3540–3544.

Grigoriev, A., R. J. Sichel, J. Y. Jo, S. Choudhury, L. Q. Chen, H. N. Lee, E. C. Landahl, B. W. Adams, E. M. Dufresne, and P. G. Evans (2009), Stability of the unswitched polarization state of ultrathin epitaxial Pb(Zr,Ti)O₃ in large electric fields, *Phys. Rev. B*, *80*(1), 6.

Grün, E., G. E. Morfill, and D. A. Mendis (1984), Dust magnetosphere interactions, in *Planetary Rings*, edited by R. Greenberg and A. Brahic, pp. 275–332 , Univ. of Ariz. Press, Tucson.

Havnes, O. (2004), Polar Mesospheric Summer Echoes (PMSE) overshoot effect due to cycling of artificial electron heating, *J. Geophys. Res.*, *109*, A02309, doi:10.1029/2003JA010159.

Havnes, O., and G. E. Morfill (1984), Effects of electrostatic forces on the vertical structure of planetary rings, *Adv. Space Res.*, *4*(9), 6.

Havnes, O., and L. I. Naesheim (2007), On the secondary charging effects and structure of mesospheric dust particles impacting on rocket probes, *Ann. Geophys.*, *25*(3), 623–637.

Havnes, O., and M. Kassa (2009), On the sizes and observable effects of dust particles in polar mesospheric winter echoes, *J. Geophys. Res.*, *114*, D09209, doi:10.1029/2008JD011276.

Havnes, O., J. Troim, T. Blix, W. Mortensen, L. I. Naesheim, E. Thrane, and T. Tonnesen (1996), First detection of charged dust particles in the Earth's mesosphere, *J. Geophys. Res.*, *101*(A5), 10,839–10,847, doi:10.1029/96JA00003.

Havnes, O., C. La Hoz, L. I. Næsheim and M. T. Rietweld (2003), First observations of the PMSE overshoot effect and its use for investigating the conditions in the summer mesosphere, *Geophys. Res. Lett.*, *30*(23), 2229, doi:10.1029/2003GL018429.

Havnes, O., C. La Hoz, M. T. Rietveld, M. Kassa, G. Baroni, and A. Biebricher (2011), Dust charging and density conditions deduced from observations of PMWE modulated by artificial electron heating, *J. Geophys. Res.*, *116*, D24203, doi:10.1029/2011JD016411.

Havnes, O., J. Gumbel, T. Antonsen, J. Hedin, and C. La Hoz (2014), On the size distribution of collision fragments of NLC dust particles and their relevance to meteoric smoke particles, *J. Atmos. Sol. Terr. Phys.*, *118*, 190–198.

Havnes, O., H. Pinedo, C. La Hoz, A. Senior, T. W. Hartquist, M. T. Rietveld, and M. J. Kosch (2015), A comparison of overshoot modelling with observations of polar mesospheric summer echoes at radar frequencies of 56 and 224 MHz, *Ann. Geophys.*, *33*(6), 737–747.

Hazarika, J., and A. Kumar (2014), Electric modulus based relaxation dynamics and ac conductivity scaling of polypyrrole nanotubes, *Synth. Met.*, *198*, 239–247.

Hervig, M. E., R. E. Thompson, M. McHugh, L. L. Gordley, J. M. Russell, and M. E. Summers (2001), First confirmation that water ice is the primary component of mesospheric clouds, *Geophys. Res. Lett.*, *28*(6), 971–974, doi:10.1029/2000GL012104.

Hervig, M. E., L. E. Deaver, C. G. Bardeen, J. M. Russell, S. M. Bailey, and L. L. Gordley (2012), The content and composition of meteoric smoke in mesospheric ice particles from SOFIE observations, *J. Atmos. Sol. Terr. Phys.*, *84–85*, 1–6.

Hunten, D. M., R. P. Turco, and O. B. Toon (1980), Smoke and dust particles of meteoric origin in the mesosphere and stratosphere, *J. Atmos. Sci.*, *37*(6), 1342–1357.

Jackson, J. D. (1962), *Classical Electrodynamics*, John Wiley, New York.

Kassa, M., O. Havnes, and E. Belova (2005), The effect of electron bite-outs on artificial electron heating and the PMSE overshoot, *Ann. Geophys.*, *23*(12), 3633–3643.

Kassa, M., M. Rapp, T. W. Hartquist, and O. Havnes (2012), Secondary charging effects due to icy dust particle impacts on rocket payloads, *Ann. Geophys.*, *30*(3), 433–439.

Kero, A., T. Bosinger, P. Pollari, E. Turunen, and M. Rietveld (2000), First EISCAT measurement of electron-gas temperature in the artificially heated D-region ionosphere, *Ann. Geophys. Atmos. Hydrospheres Space Sci.*, *18*(9), 1210–1215.

Knappmiller, S., S. Robertson, Z. Sternovsky, and M. Friedrich (2008), A rocket-borne mass analyzer for charged aerosol particles in the mesosphere, *Rev. Sci. Instrum.*, *79*(10), 10.

Kolikov, K., D. Ivanov, G. Krastev, Y. Epitropov, and S. Bozhkov (2012), Electrostatic interaction between two conducting spheres (vol 70, pg 91, 2012), *J. Electrost.*, *70*(5), 468–468.

Konopka, U., G. E. Morfill, and L. Ratke (2000), Measurement of the interaction potential of microspheres in the sheath of a rf discharge, *Phys. Rev. Lett.*, *84*(5), 891–894.

La Hoz, C., and O. Havnes (2008), Artificial modification of polar mesospheric winter echoes with an RF heater: Do charged dust particles play an active role?, *J. Geophys. Res.*, *113*, D19205, doi:10.1029/2008JD010460.

Lange, M. A., and T. J. Ahrens (1983), The dynamic tensile-strength of ice and ice-silicate mixtures, *J. Geophys. Res.*, *88*(NB2), 1197–1208, doi:10.1029/JB088iB02p01197.

Litwin, K. L., B. R. Zygielbaum, P. J. Polito, L. S. Sklar, and G. C. Collins (2012), Influence of temperature, composition, and grain size on the tensile failure of water ice: Implications for erosion on Titan, *J. Geophys. Res.*, *117*, E08013, doi:10.1029/2012JE004101.

Lübken, F. J., and J. Höffner (2004), Experimental evidence for ice particle interaction with metal atoms at the high latitude summer mesopause region, *Geophys. Res. Lett.*, *31*, L08103, doi:10.1029/2004GL019586.

Lübken, F. J., M. Rapp, and P. Hoffmann (2002), Neutral air turbulence and temperatures in the vicinity of polar mesosphere summer echoes, *J. Geophys. Res.*, *107*(D15), 4273, doi:10.1029/2001JD000915.

Mahmoudian, A., and W. A. Scales (2012), Temporal evolution of radar echoes associated with mesospheric dust clouds after turn-on of radio wave heating, *J. Geophys. Res.*, *117*, D06221, doi:10.1029/2011JD017166.

Mahmoudian, A., W. A. Scales, M. J. Kosch, A. Senior, and M. Rietveld (2011), Dusty space plasma diagnosis using temporal behavior of polar mesospheric summer echoes during active modification, *Ann. Geophys.*, *29*(11), 2169–2179.

Markes, M. E., and P. F. Williams (2000), The electrostatic interaction of charged, dust-particle pairs in plasmas, *Phys. Lett. A*, *278*(3), 152–158.

Megner, L., M. Rapp, and J. Gumbel (2006), Distribution of meteoric smoke—Sensitivity to microphysical properties and atmospheric conditions, *Atmos. Chem. Phys.*, *6*, 4415–4426.

Megner, L., J. Gumbel, M. Rapp, and D. E. Siskind (2008), Reduced meteoric smoke particle density at the summer pole—Implications for mesospheric ice particle nucleation, *Adv. Space. Res.*, *41*, 41–49.

Mendis, D. A., and M. Horányi (2013), Dusty plasma effects in comets: Expectations for Rosetta, *Rev. Geophys.*, *51*, 53–75, doi:10.1002/rog.20005.

Munirov, V. R., and A. V. Filippov (2013), Interaction of two dielectric macroparticles, *J. Exp. Theor. Phys.*, *117*(5), 809–819.

Næsheim, L. I., O. Havnes, and C. La Hoz (2008), A comparison of polar mesosphere summer echo at VHF (224 MHz) and UHF (930 MHz) and the effects of artificial electron heating, *J. Geophys. Res.*, *113*, D08205, doi:10.1029/2007JD009245.

Öpik, E. J. (1956), Interplanetary dust and terrestrial accretion of meteoric matter, *Irish Astron. J.*, *4*, 84.

Pat-El, I., D. Laufer, G. Notesco, and A. Bar-Nun (2009), An experimental study of the formation of an ice crust and migration of water vapor in a comet's upper layers, *Icarus*, *201*(1), 406–411.

Pedersen, A., J. Troim, and J. Kane (1969), Rocket measurement showing removal of electrons above the mesopause in summer at high latitudes, *Planet. Space Sci.*, *18*, 3.

Plane, J. M. C. (2004), A time-resolved model of the mesospheric Na layer: Constraints on the meteor input function, *Atmos. Chem. Phys.*, *4*, 627–638.

Rapp, M. (2009), Charging of mesospheric aerosol particles: The role of photodetachment and photoionization from meteoric smoke and ice particles, *Ann. Geophys.*, *27*(6), 2417–2422.

Rietveld, M. T., H. Kohl, and H. Kopka (1993), Introduction to ionospheric heating at Tromsø: 1. Experimental overview, *J. Atmos. Terr. Phys.*, *55*, 577–599.

Robertson, S., et al. (2009), Mass analysis of charged aerosol particles in NLC and PMSE during the ECOMA/MASS campaign, *Ann. Geophys.*, *27*(3), 1213–1232.

Scales, W. A. (2004), Electron temperature effects on small scale plasma irregularities associated with charged dust in the Earths mesosphere, *IEEE Trans. Plasma Sci.*, *32*, 7.

Scales, W. A., and C. Chen (2008), On the initial perturbation of mesospheric, dust associated irregularities by high powered radio waves, *Adv. Space Res.*, *41*(1), 50–56.

Seizinger, A., R. Speith, and W. Kley (2013), Tensile and shear strength of porous dust agglomerates, *Astron. Astrophys.*, *559* A19, doi:10.1051/0004-6361/201322046.

Selwyn, G. S., J. E. Heidenreich, and K. L. Haller (1990), Particle trappint phenomena in radio-frequency plasmas, *Appl. Phys. Lett.*, *57*(18), 1876–1878.

Senior, A., A. Mahmoudian, H. Pinedo, C. La Hoz, M. T. Rietveld, W. A. Scales, and M. J. Kosch (2014), First modulation of high-frequency polar mesospheric summer echoes by radio heating of the ionosphere, *Geophys. Res. Lett.*, *41*, 5347–5353, doi:10.1002/2014GL060703.

She, C. Y., B. P. Williams, P. Hoffmann, R. Latteck, G. Baumgarten, J. D. Vance, J. Fiedler, P. Acott, D. C. Fritts, and F. J. Lübken (2006), Simultaneous observation of sodium atoms, NLC and PMSE in the summer mesopause region above ALOMAR, Norway (69°N, 12°E), *J. Atmos. Sol. Terr. Phys.*, *68*(1), 93–101.

Warren, S. G. (1984), Optical constants of ice from the ultraviolet to the microwave, *Appl. Opt.*, *23*, 1206–1225.

Zhukov, S., H. Kungl, Y. A. Genenko, and H. von Seggern (2014), Statistical electric field and switching time distributions in PZT 1Nb2Sr ceramics: Crystal- and microstructure effects, *J. Appl. Phys.*, *115*(1), 13.